npg

INVITED ARTICLE

Morphological changes of isotactic poly(methyl methacrylate) thin films via self-organization and stereocomplex formation

Daisuke Kamei[1], Hiroharu Ajiro[1,2] and Mitsuru Akashi[1,2]

Morphological changes of macromolecularly porous thin films during isotactic (*it*) poly(methyl methacrylate) (PMMA) crystallization and the subsequent syndiotactic (*st*) poly(methacrylic acid) (PMAA) incorporation are described herein. Porous *it*-PMMA thin films were prepared on a gold substrate by the selective extraction of *st*-PMAA from stereocomplex films composed of *it*-PMMA/*st*-PMAA using layer-by-layer assembly. *it*-PMMA crystallization occurred when the porous *it*-PMMA films were immersed in a mixed solvent of acetonitrile/water (4/6, v/v). Surface analyses of films were performed by scanning electron microscopy, atomic force microscopy, X-ray photoelectron spectroscopy (XPS) and static contact angles. Dotted aggregates of *it*-PMMA appeared on crystallized films, whereas networks composed of crystallized *it*-PMMA and the stereocomplex were observed on *st*-PMAA incorporated films. Gold substrate peaks were observed not on porous *it*-PMMA films, but on crystallized *it*-PMMA films by XPS, indicating that homogeneously broadened *it*-PMMA in porous films was localized because of its crystallization. The static contact angle of crystallized *it*-PMMA films was $36.5 \pm 1.6^\circ$, which was smaller than that of porous *it*-PMMA films ($49.2 \pm 1.9^\circ$). This difference resulted from the surface morphology of the thin films. Dotted *it*-PMMA aggregates were also observed when spin-coated films were immersed in the mixed solvent.

INTRODUCTION

Stereoregular poly(methyl methacrylate)s (PMMA) have attracted much attention because of their unique crystalline structure, morphology, and other particular properties since the first report by Stroupe and coworkers.[1] Isotactic (*it*) PMMA and syndiotactic (*st*) PMMA can self-aggregate either by themselves or as stereocomplexes. *it*-PMMA crystals form a double-stranded helical structure,[2] whereas *st*-PMMA does not crystallize, but includes specific organic solvents in a cavity within its single-stranded helix.[3] The stereoregular PMMA stereocomplex is a complementary helical structure formed on the basis of structural fitting between two chains of *it*-PMMA and *st*-PMMA.[4–6] Recently, the discussion has arisen on the basic structure of the PMMA stereocomplex by using X-ray[7] and atomic force microscopy (AFM),[8,9] although it was concluded that the structure of the stereocomplex is a helix with *it*-PMMA on the inside surrounded by *st*-PMMA.

Interfacial rearrangements of *it*-PMMA chains are expected to occur more easily than *st*-PMMA or atactic-PMMA chains, because the glass transition temperature of *it*-PMMA ($\sim 40\,^\circ$C) is significantly lower than that of *st*-PMMA or atactic-PMMA (around 105–$135\,^\circ$C).[10] The crystallization of *it*-PMMA films has been researched by annealing at elevated temperatures for more than a few days, or under compres-

sion.[11–19] Most of these studies focused mainly on structural analyses of the crystals using infrared (IR) spectroscopy and X-ray diffraction (XRD), but the morphology of crystallized *it*-PMMA films has also been studied for a long time.[11,12,16,18] The film-formation methods used were either solvent evaporation from solution-cast films or the Langmuir–Blodgett technique as described below. Over 30 years ago, Klement and Geil[11] studied the lamellar growth of *it*-PMMA cast films annealed at a narrow temperature range (55–65 °C) with electron microscopy, whereas Challa and coworkers[12] observed the macroscopic hexagonal structures of crystallized *it*-PMMA from casts at 90–130 °C using a polarization microscope. Later, Brinkhuis and Schouten[16] demonstrated the epitaxial crystallization in *it*-PMMA cast films covered by Langmuir–Blodgett overlayers. Recently, Yashima and coworkers[18] directly observed two-dimensional folded-chain crystals of *it*-PMMA monolayers obtained by Langmuir–Blodgett deposition using AFM.

In contrast, macromolecularly porous *it*-PMMA thin films have been studied as a scientifically important model, as they have strictly controlled nanospaces and were utilized for specific molecular recognition or precise reaction fields by forming stereocomplexes on substrates.[20–25] Porous *it*-PMMA thin films were prepared on quartz

[1]Department of Applied Chemistry, Graduate School of Engineering, Osaka University, 2–1 Yamada-oka, Suita, Osaka, Japan and [2]The Center for Advanced Medical Engineering and Informatics, Osaka University, 2–2 Yamada-oka, Suita, Osaka, Japan
Correspondence: Dr M Akashi, Department of Applied Chemistry, Graduate School of Engineering, Osaka University, 2–1 Yamada-oka, Suita, Osaka 565–0871, Japan.
E-mail: akashi@chem.eng.osaka-u.ac.jp

crystal microbalance (QCM), silica or glass substrates through layer-by-layer (LbL) assembly[26] of *it*-PMMA/*st*-poly(methacrylic acid) (PMAA)[27–29] and the selective extraction of *st*-PMAA from *it*-PMMA/*st*-PMAA stereocomplex films, taking advantage of the different solubilities of each component polymer. The *it*-PMMA/*st*-PMAA stereocomplex also forms a double-stranded helix similar to the aforementioned *it*-PMMA/*st*-PMMA stereocomplex.[30] In addition, porous films prepared by LbL assembly have been compared with spin-coated *it*-PMMA films. The spin-coated films showed neither the specific recognition of *st*-polymethacrylate[20] nor the template polymerization of methacrylic acid.[22] Thus, it is concluded that these phenomena are particular to the macromolecularly porous films.

More recently, we observed partial *it*-PMMA crystallization, as well as *st*-PMAA incorporation, into porous films by XRD analyses.[31,32] It was revealed that crystallized *it*-PMMA chains in films formed double-stranded helices.[2,33] The crystallization of *it*-PMMA occurred merely by immersing the porous films in a mixed solvent of acetonitrile/water (4/6, v/v) at room temperature, which is a different procedure and milder than conventional conditions.[11–19] Furthermore, *st*-PMAA incorporation into porous *it*-PMMA films was analyzed at the molecular level by QCM. Porous *it*-PMMA films incorporated *st*-PMAA with increasing acetonitrile content in the *st*-PMAA solution. Therefore, it was concluded that acetonitrile was important for *it*-PMMA chain motion in porous films. *st*-PMAA was also incorporated into *it*-PMMA films driven by stereocomplex formation, even after *it*-PMMA crystallized partially, although the amount of *st*-PMAA incorporated into crystallized films was reduced as compared with the incorporation into porous films.[32] However, both the changes in the morphology or properties of the films and the mechanisms responsible for these phenomena remained unclear.

In this study, we focused on the morphological changes of porous thin films during *it*-PMMA crystallization and the subsequent *st*-PMAA incorporation. Films were characterized by scanning electron microscopy (SEM), AFM, X-ray photoelectron spectra and static contact angles. We also investigated whether the morphological changes of spin-coated films occur after immersion into a mixed solvent of acetonitrile/water in order to study the mechanisms of these interfacial rearrangements.

EXPERIMENTAL PROCEDURE
Materials
it-PMMA[34] (M_n=22 900, M_w/M_n=1.21, *mm*:*mr*:*rr*=96:2:2) and *st*-PMAA[35] (M_n=33 700, M_w/M_n=1.45, *mm*:*mr*:*rr*=1:5:94) were synthesized by conventional anionic polymerization. The number average molecular weights and distributions were measured by size exclusion chromatography using PMMA standards with a tetrahydrofuran eluant at 40 °C and a flow rate of 0.6 ml min^{-1}. Tacticities were analyzed from α-methyl proton signals using 400-MHz nuclear magnetic resonance (nitrobenzene-d_5, 110 °C). Characterization of *st*-PMAA was achieved after the carboxyl group was methylated. Acetonitrile was purchased from Wako Pure Chemical Industries (Osaka, Japan). Ultrapure distilled water was provided by the MILLI-Q laboratory system (Millipore, Billerica, MA, USA).

Film preparation
An AT-cut QCM with a parent frequency of 9 MHz was obtained from USI (Fukuoka, Japan) and used as the substrate. Frequency was monitored by an Iwatsu frequency counter (Model 53131A: Iwatsu Test Instruments Corp., Tokyo, Japan). The quartz crystal (9 mm diameter) was coated on both sides with mirror-like polished gold electrodes (4.5 mm in diameter). At first, the QCM electrode was cleaned three times with a piranha solution, a mixed aqueous solution of H_2SO_4/40% H_2O_2 (3/1, v/v) for 1 min, followed by rinsing with ultrapure water and drying with N_2 gas. LbL films were prepared as

follows: the substrate was alternatively immersed into an *it*-PMMA acetonitrile solution and an *st*-PMAA acetonitrile/water (4/6, v/v) solution at a concentration of 0.017 unitM for 5 min at 25 °C each. The substrate was rinsed with each solvent, and dried with N_2 gas whenever it was taken out from each solution. This alternative deposition step was repeated 16 times to fabricate stereocomplexes of *it*-PMMA/*st*-PMAA on the substrates. Porous *it*-PMMA thin films were prepared by immersion into a 10 mM NaOH aqueous solution. The porous films were immersed in mixed solvents of acetonitrile/water (4/6, v/v) for 10 h, and then immersed in *st*-PMAA solutions of mixed acetonitrile/water (4/6, v/v) solvents for 115 min.[32] Spin-coated *it*-PMMA films were prepared on the QCM at 1500 r.p.m. for 1 min with 0.051 unitM *it*-PMMA chloroform solutions. Acetonitrile was not used because it was a poor solvent for PMMA[10] and could not dissolve *it*-PMMA completely at more than 0.017 unitM. Thus, chloroform, a good solvent for PMMA, was used to prepare the spin-coated films. The amount of *it*-PMMA adsorbed onto the substrate was approximately −1600 Hz per QCM. Spin-coated films were then immersed in acetonitrile/water (4/6, v/v) for 10 h.

Measurements
SEM images were obtained with a JSM-6701F (JEOL, Akishima, Japan) at an acceleration voltage of 5 kV after osmium tetraoxide was spattered onto the surfaces of films at a thickness of approximately 5 nm. AFM images were obtained with a JSPM-5400 (JEOL) that was operated in tapping mode in air at 25 °C. Scanning was performed using silicon cantilevers (NSC35, μ-masch; resonance frequency: around 150 kHz; spring constant: 4.5 N m^{-1}) within an area of 5×5 μm^2 with a 512 scan line and a scan speed of 5.0 μm s^{-1}. We did not perform any image processing other than the flat leveling. The mean square roughness (R_a) in the observed areas was estimated from the following equation, where $F(x,y)$ is the surface relative to the center plane, which is a flat plane parallel to the mean plane, and L_x and L_y are the dimensions of the surface.

$$R_a = 1/(L_x L_y) \int_0^{L_x} \int_0^{L_y} |F(x,y)| \, dx \, dy$$

X-ray photoelectron spectroscopy (XPS) was obtained with a spectrometer (AXIS 165, Shimadzu-Kratos, Kyoto, Japan) using MgKα radiation. The typical operating conditions were as follows: X-ray gun, 12 kV, 10 mA; takeoff angle, 90 °C; pressure in the source chamber, ∼10^{-9} torr. The static contact angles of the thin films were measured by dropping ultrapure water on the films at 25 °C with a DropMaster 500 (Kyowa InterFACE Science, Niiza, Japan). Contact angles were determined 10 s after applying the drop. The volume of water in the drop was 0.5 μl. All reported values represent the average of at least six measurements taken at different locations on the film surface.

RESULTS AND DISCUSSION
We used QCM analysis to calculate the amount of *it*-PMMA assembled on the gold substrate by Sauerbrey's equation.[36] A typical QCM analysis is shown in Figure 1, and the time evolution means the period of immersion time in each solution or solvent. The stepwise stereocomplex assembly of *it*-PMMA/*st*-PMAA and the selective extraction of *st*-PMAA from assembled films were confirmed in previous papers.[20,23,25,32] Interestingly, the elution of porous *it*-PMMA thin films was barely observed after the films were immersed into acetonitrile/water (4/6, v/v) for 10 h, although the crystallized *it*-PMMA peaks were observed by XRD.[31,32] These results indicate that the interfacial rearrangements of *it*-PMMA chains that occurred in films were driven by the mixed solvent, whereas *it*-PMMA crystallization was driven by annealing at high temperature or under compression in previous studies.[11–19] The crystallized *it*-PMMA thin films can incorporate *st*-PMAA, most likely because further interfacial rearrangements also occurred in these films. Therefore, the morphological changes of the porous thin films during *it*-PMMA crystallization and the subsequent *st*-PMAA incorporation were initially

analyzed by SEM and AFM. The same crystallized *it*-PMMA films, which corresponded to approximately −1400 Hz per QCM, and the *st*-PMAA incorporated films were used in SEM and AFM observation.

We have observed several hemispherical outshoots on the surface of crystallized *it*-PMMA films by AFM,[32] which implies that the morphological changes of the films occurred in a wide area as compared with the scanning area (1×1 μm) used in previous studies.[20,29,32] Thus, SEM was used to observe the macroscopic deformation of porous thin films during *it*-PMMA crystallization and the subsequent
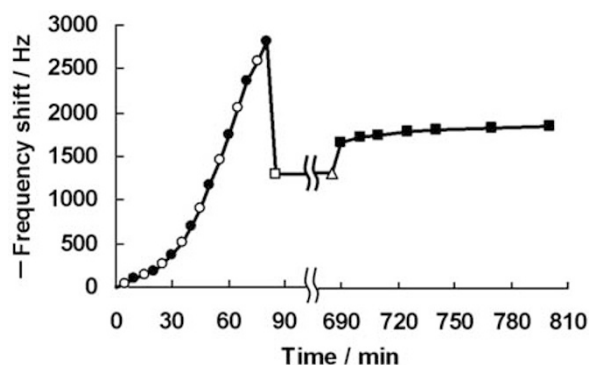
Figure 1 Typical QCM analysis of the layer-by-layer assembly, *st*-PMAA extraction, isotactic *it*-PMMA crystallization and subsequent *st*-PMAA incorporation. *it*-PMMA (white circles) in acetonitrile and *st*-PMAA (black circles) in acetonitrile/water (4/6, v/v) were alternately assembled on a QCM substrate at 0.017 unitM at 25 °C. Porous *it*-PMMA films were prepared using 10 mM NaOH(aq) (white square). The following *it*-PMMA crystallization occurred in a mixed solvent of acetonitrile/water (4/6, v/v) (white triangle). The last *st*-PMAA incorporation was observed at 0.017 unitM at 25 °C (black squares).
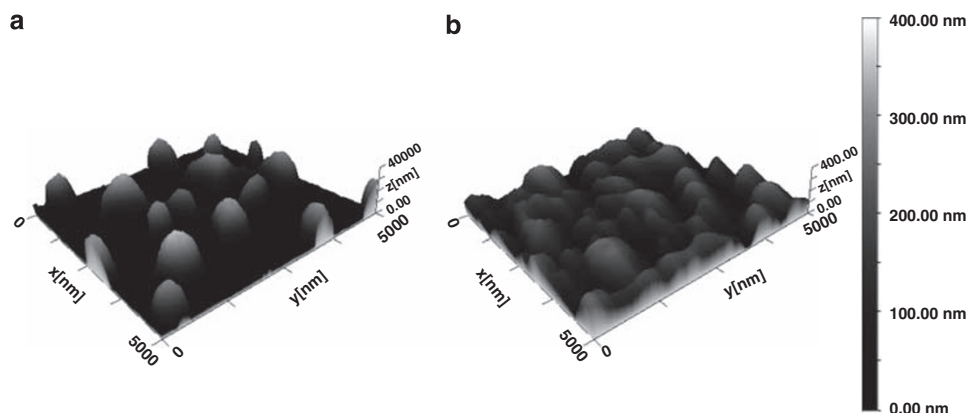
st-PMAA incorporation. Figure 2 shows SEM images of crystallized *it*-PMMA films and *st*-PMAA incorporated films after 10 h of immersion in acetonitrile/water (4/6, v/v). Dotted aggregates of crystallized *it*-PMMA and networks of the *it*-PMMA/*st*-PMAA mixed assembly broadened evenly at the submillimeter scale (Figures 2a and b). The patterns were not observed on the surface of a bare QCM substrate and porous *it*-PMMA films (Supplementary Figure S1). In the magnified view (tilted at 40-degree angles), some dots were connected to form big outshoots on the crystallized *it*-PMMA films (Figure 2c), and some isolated outshoots were also observed on *st*-PMAA incorporated films after *it*-PMMA crystallization (Figure 2d). However, most regions of the crystallized *it*-PMMA films and *st*-PMAA-incorporated films formed dots and networks, respectively, although the configurations of these assemblies cannot be controlled yet. This morphological change from dots to networks likely resulted from an increased polymer density of films during the incorporation of *st*-PMAA.

AFM analysis was used to calculate both the height of the assemblies and the surface roughness of films, which was difficult to measure by SEM. Figure 3 shows AFM images of crystallized *it*-PMMA films and *st*-PMAA incorporated films after *it* PMMA crystallization. Hemispherical outshoots of crystallized *it* PMMA, which were several hundred nanometers high, were arranged in a dot pattern on films (Figure 3a), whereas porous films were relatively flat (Supplementary Figure S2). The mean square roughness (R_a) of the crystallized *it*-PMMA films was 53 nm, although the R_a of the smooth parts (0.3×0.3 μm) of films was 3.3 ± 0.2 nm (n=3). This value was more similar to that of a bare QCM substrate (3.1 nm) than that of porous *it*-PMMA films (17 nm) (Supplementary Figure S2), suggesting that the bare gold surface is exposed. In addition, the outshoots of crystallized *it*-PMMA films, which corresponded to approximately −700 Hz per QCM (Supplementary Figure S2), were smaller and more
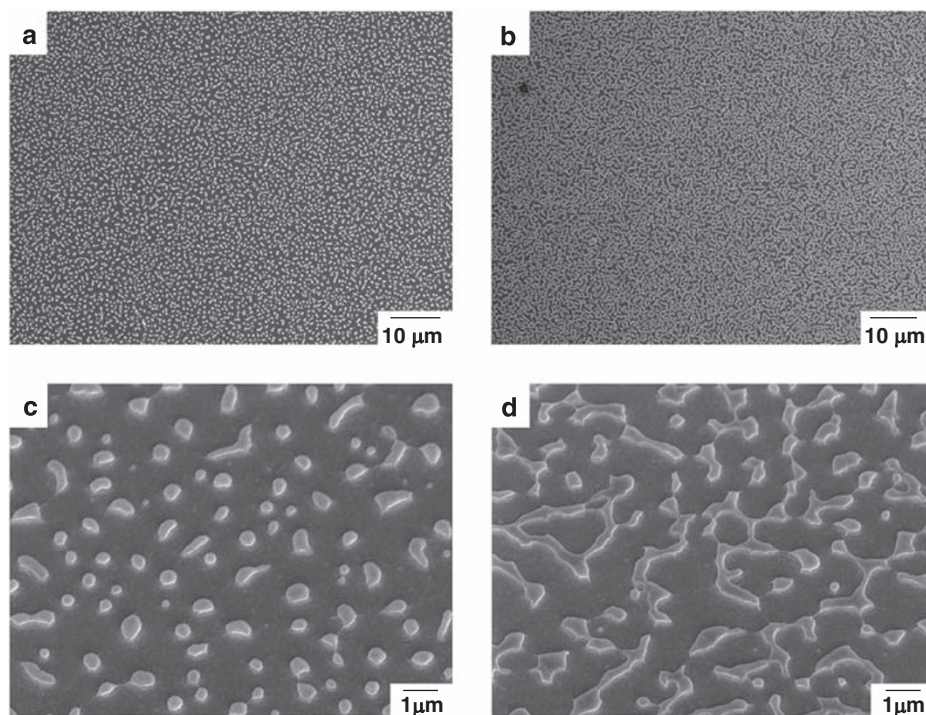
Figure 2 SEM images of crystallized *it*-PMAA films (**a**, **c**) and *st*-PMAA incorporated films (**b**, **d**) after 10 h of immersion in acetonitrile/water (4/6, v/v). (**a**, **b**) Top view. (**c**, **d**) Tilted view.
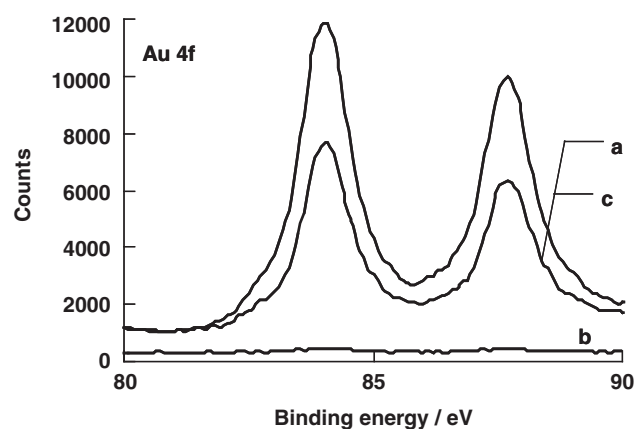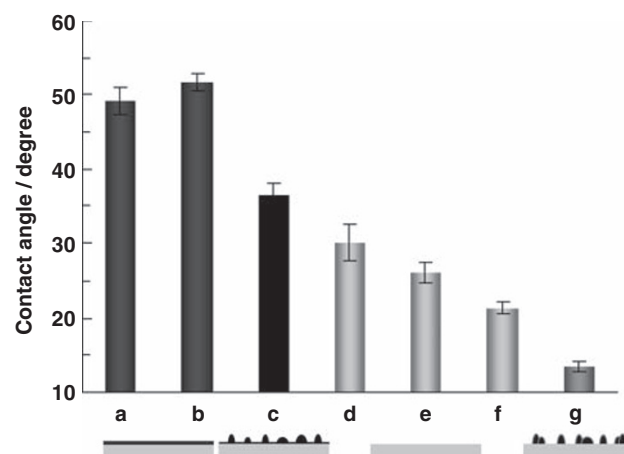
Figure 3 AFM images of crystallized *it*-PMAA films (**a**) and *st*-PMAA incorporated films (**b**) after 10 h of immersion in acetonitrile/water (4/6, v/v).

than that of the crystallized films in Figure 3a (-1400 Hz per QCM), which implies that film thickness is one of the important parameters for morphological changes of *it*-PMMA films. Furthermore, a similar dot pattern was also observed on crystallized *it*-PMMA (-700 Hz per QCM) after 40 h of immersion in acetonitrile/water (4/6, v/v) (Supplementary Figure S2). On the other hand, networks of agglomerates composed of crystallized *it*-PMMA and stereocomplexes were observed on the surface of *st*-PMAA incorporated films (Figure 3b), and the heights of these assemblies were not significantly different from that of crystallized *it*-PMMA films. Therefore, the polymer chains in films likely spread in a horizontal direction during *st*-PMAA incorporation. Indeed, the R_a of *st*-PMAA-incorporated films was 46 nm, but the R_a of the smooth parts (0.3×0.3 μm) was 3.8 ± 0.5 nm ($n=3$). This morphological change in films indicated that some noncrystalline parts of *it*-PMMA could incorporate *st*-PMAA, and that a rearrangement of the partially crystallized *it*-PMMA might occur on the film surface.

Next, we were interested in the changes in properties of porous *it*-PMMA films. The deformation of films during *it*-PMMA crystallization would dynamically change the film thickness. XPS analysis is a common tool to confirm chemical bonds on a surface at ~ 10 nm of the measured depth. The XPS spectra of a bare QCM substrate, porous *it*-PMMA films and crystallized *it*-PMMA films are shown in Figure 4. Distinct Au 4f peaks at around 84.1 and 87.7 eV were observed on the QCM substrate (Figure 4a). In contrast, these Au peaks were not observed on the surface of porous films (Figure 4b), showing that the thickness of porous films was more than 10 nm, and that the substrate was evenly covered with film. In a previous paper,[20] the thickness of porous *it*-PMMA films was determined to be 44 nm by AFM scratching mode, which corresponded to approximately -800 Hz per QCM. Therefore, *it*-PMMA film thickness was calculated as 83 nm (-1500 Hz per QCM) in this study (Figure 1), according to a constant rate of 0.055 nm/Hz. Note that the intensity of Au 4f peaks on the surface of crystallized *it*-PMMA films was about two-thirds of that of the QCM substrate (Figure 4c), and that the heights of the outshoots on the crystallized *it*-PMMA films reached several hundred nanometers (Figure 3a), where Au peaks should not be detected. Thus, the film thickness of the smooth parts became less than 10 nm after *it*-PMMA films were immersed in acetonitrile/water (4/6, v/v). These results confirmed that the homogeneously broadened *it*-PMMA in porous films became localized because of its crystallization, which brought about differences in the polymer density of films.


Figure 4 XPS in the region of the gold element of a bare quartz crystal microbalance substrate (**a**), porous *it*-PMMA films (**b**) and crystallized *it*-PMMA films (**c**) after 10 h of immersion in acetonitrile/water (4/6, v/v).

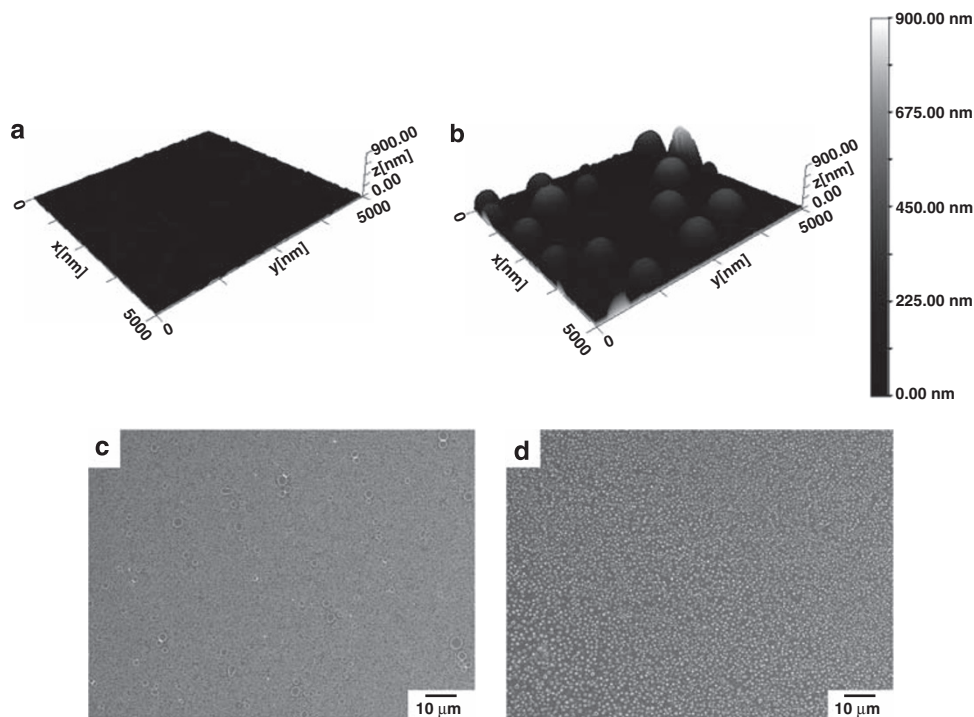**Figure 5** Static contact angles of porous *it*-PMMA films as prepared (**a**) and after 10 h of immersion in water (**b**), crystallized *it*-PMMA films after 10 h of immersion in acetonitrile/water (4/6, v/v) (**c**), stereocomplex films (**d**) and *st*-PMAA incorporated films just after *st*-PMAA extraction (**e**) and after 10 h of immersion in water (**f**) and acetonitrile/water (4/6, v/v) (**g**).

Furthermore, film characteristics were analyzed on the millimeter scale with static contact angles, which have been used to confirm stepwise stereocomplex formation during LbL assembly.[29] We thought that the contact angles of each film would change according to its surface components or shapes. Figure 5 shows the dependence of static contact angles on various film surfaces. Surface components and polymer conformations were analyzed by attenuated total reflection-IR (Supplementary Figure S3).[20] The mean angles of porous *it*-PMMA films as prepared and after 10 h of immersion in water were $49.2 \pm 1.9°$ and $51.7 \pm 1.0°$, respectively (Figures 5a and b). This is reasonable because XRD analyses revealed that no structural

changes of porous *it*-PMMA films occurred in water.[32] In contrast, the angles of crystallized *it*-PMMA films after 10 h immersion in acetonitrile/water (4/6, v/v) was $36.5 \pm 1.6°$ (Figure 5c). These differences likely resulted from a surface morphology change of the thin films, because both films were composed only of *it*-PMMA and the two porous films were smooth compared with crystallized films (Figure 3a, Supplementary Figure S2). We should also consider that the film thickness of the smooth parts in crystallized *it*-PMMA films was less than 10 nm and the gold surface of QCM is exposed, according to XPS results (Figure 4c). Although the mean angle of a bare QCM substrate was $69.2 \pm 1.4°$, Burton and Bhushan[37] reported
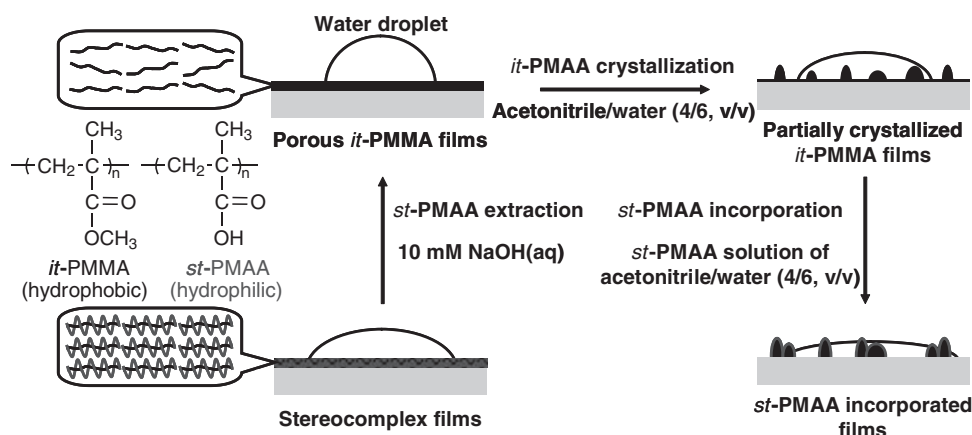
Figure 6 Schematic illustration of the morphological changes of macromolecularly porous thin films in *it*-PMMA crystallization and *st*-PMAA incorporation.

Figure 7 AFM and SEM images of spin-coated *it*-PMMA films prepared from a chloroform solution (**a**, **c**) and after 10 h of immersion in acetonitrile/water (4/6, v/v) (**b**, **d**).

that increasing roughness on hydrophilic surfaces, such as the patterned PMMA surface, decreased the contact angle, which was consistent with these results.

This tendency was also observed in the case of stereocomplex films. The contact angle of the original LbL films was $30.2 \pm 2.5°$, and the angles of *st*-PMAA incorporated films after *st*-PMAA extraction and a subsequent 10 h of immersion in water were $26.4 \pm 1.3°$ and $21.4 \pm 0.8°$, respectively (Figures 5d—f). The mean values of stereocomplex films were smaller than those of porous *it*-PMMA films,[29] because the hydrophobic *it*-PMMA is buried in the helical structure of hydrophilic *st*-PMAA in the stereocomplex model.[30] *st*-PMAA incorporated films remained flat (Supplementary Figure S2), although the slow crystallization of *it*-PMMA also occurred during the incorporation of *st*-PMAA.[31] Therefore, the fast *st*-PMMA incorporation by stereocomplexation might prevent film deformation because of *it*-PMMA crystallization. On the other hand, the angle of *st*-PMAA incorporated films after *it*-PMMA crystallization was $13.6 \pm 0.7°$ (Figure 5g). It is indicated that the surface of films was covered with stereocomplexes (Figure 6), although the *it*-PMMA inside the aggregates is densely packed and loses the ability to incorporate *st*-PMAA. It also remains unclear whether *st*-PMAA adsorbed both on the crystallized *it*-PMMA outshoots and on the smooth domains of films. These tendencies of static contact angles also corresponded to the relatively regular surface profile at the submillimeter scale, which was observed by SEM (Figures 2a and b).

We were also interested in whether ordinary *it*-PMMA films would form outshoots after immersion into a mixed solvent of acetonitrile/water. Spin-coated *it*-PMMA films were prepared on the QCM substrate from the chloroform solution as described in the experimental procedure section. Figure 7 shows the AFM and SEM images of spin-coated *it*-PMMA films as prepared and after immersed in acetonitrile/water (4/6, v/v) for 10 h. The R_a of spin-coated films was 8.4 nm and the film surface was relatively smooth (Figure 7a). A few big craters were formed on the films, most likely because of the evaporation of chloroform (Figure 7c). The QCM frequency shift was a few hertz after 10 h of immersion in acetonitrile/water (4/6, v/v), which implies that the spin-coated films did not dissolve in the mixed solvent either. Semispherical outshoots were also observed on films after immersion (Figure 7b), and dotted aggregates of *it*-PMMA broadened evenly at the submillimeter scale (Figure 7d). The same tendency of crystallized *it*-PMMA films was obtained by LbL assembly, even though the R_a of films (82 nm) was much greater than that of *it*-PMMA films from LbL assembly (32 nm). The surface roughness derived by the crystallization of *it*-PMMA is dependent on the initial thickness, roughness or morphology of the films, such as the cratered surface. These results indicate that the formation of these hemispherical outshoots would occur by rearrangements of *it*-PMMA chains in thin films.

CONCLUSIONS

We investigated the morphological changes of porous thin films on a QCM substrate during *it*-PMMA crystallization and the subsequent *st*-PMAA incorporation. Dotted aggregates of crystallized *it*-PMMA appeared on films on SEM and AFM images, although the films were not dissolved in a mixed solvent of acetonitrile/water. Gold substrate peaks were observed on crystallized *it*-PMMA films by XPS. Therefore, this indicated that the adsorbed *it*-PMMA spontaneously localized in films to reform the surface profile. These dotted *it*-PMMA aggregates were also observed when spin-coated films were immersed in the mixed solvent, suggesting that this immersion method is a simple and different approach to film deformation, as compared with previous

studies. On the other hand, networks of crystallized *it*-PMMA and the stereocomplex appeared on *st*-PMAA-incorporated films. In this way, the design and restructuring of self-assembled films at the nano or micrometer scale were achieved through self-organization and stereocomplex formation of stereoregular polymethacrylates.

1 Fox, T. G., Garret, B. S., Goode, W. E., Grantch, S., Kincaid, J. F. & Spell, A. Crystalline polymers of methyl methacrylate. *J. Am. Chem. Soc.* **80,** 1768–1769 (1958).

2 Kusanagi, H., Tadokoro, H. & Chatani, Y. Double stranded helix of isotactic poly(methyl methacrylate). *Macromolecules* **9,** 531–532 (1976).

3 Kusuyama, H., Takase, M., Higashihata, Y., Tseng, H. T., Chatani, Y. & Tadokoro, H. Structural change of st-PMMA on drawing, absorption, and desorption of solvents. *Polymer* **23,** 1256–1258 (1982).

4 Spevacek, J. & Schneider, B. Aggregation of stereoregular poly(methyl methacrylates). *Adv. Colloid Interface Sci.* **27,** 81–150 (1987).

5 te Nijenhuis, K. Thermoreversible networks. 4. poly (methyl methacrylate). *Adv. Polym. Sci.* **130,** 67–81 (1997).

6 Hatada, K. & Kitayama, T. Structurally controlled polymerizations of methacrylates and acrylates. *Polym. Int.* **49,** 11–47 (2000).

7 Schomaker, E. & Challa, G. Complexation of stereoregular poly(methyl methacrylates). 14. The basic structure of the stereocomplex of isotactic and syndiotactic poly(methyl methacrylate). *Macromolecules* **22,** 3337–3341 (1989).

8 Liu, J., Zhang, Y., Zhang, J., Shen, D., Guo, Q. Takahashi, I. & Yan, S. Stereocomplexation and monolayer morphologies of a stereoregular poly(methyl methacrylate) mixture formed at the air/water surface. *J. Phys. Chem. C* **111,** 6488–6494 (2007).

9 Kumaki, J., Kawauchi, T., Okoshi, K., Kusanagi, H. & Yashima, E. Supramolecular herical structure of the stereocomplex composed of complementary isotactic and syndiotactic poly(methyl methacrylate)s as revealed by atomic force microscopy. *Angew. Chem. Int. Edn. Engl.* **46,** 5348–5351 (2007).

10 Wunderlich, W. in *Polymer Handbook* (eds. Brandrup, J. & Immergut, E. H.) Ch. 5, V77–V80 (John Wiley & Sons, New York, 1989).

11 Klement, J. J. & Geil, P. H. Deformation and annealing behavior. 3. Thin films of polycarbonate, isotactic polymethyl methacrylate, and isotactic polystyrene. *J. Macromol. Sci. B* **6,** 31–56 (1972).

12 de Boer, A., van Ekenstein, G. O. R. A. & Challa, G. Crystallization of isotactic poly(methyl methacrylate) from the melt. *Polymer* **16,** 930–932 (1975).

13 Schneider, B., Stokr, J., Spevacek, J. & Baldrian, J. Infrared spectra and crystallinity of isotactic poly(methyl methacrylate) and of its deuterated analogues. *Makromol. Chem.* **188,** 2705–2711 (1987).

14 Dybal, J. & Krimm, S. Normal-mode analysis of infrared and raman spectra of crystalline isotactic poly(methyl methacrylate). *Macromolecules* **23,** 1301–1308 (1990).

15 Brinkhuis, R. H. R. & Schouten, A. J. Thin-film behavior of poly(methyl methacrylates). 2. An FT-IR study of Langmuir-Blodgett films of isotactic PMMA. *Macromolecules* **24,** 1496–1504 (1991).

16 Brinkhuis, R. H. R. & Schouten, A. J. Thin-film behavior of poly(methyl methacrylates). 3. Epitaxial crystallization in thin films of isotactic poly(methyl methacrylate) using crystalline Langmuir-Blodgett layers. *Macromolecules* **25,** 2717–2724 (1992).

17 Zhou, D., Li, L., Che, B., Cao, Q., Lu, Y. & Xue, G. Metastable isotactic poly(methyl methacrylate) prepared by freeze-extracting solutions in poly(ethylene glycol). *Macromolecules* **37,** 4744–4747 (2004).

18 Kumaki, J., Kawauchi, T. & Yashima, E. Two-demensional folded chain crystals of a synthetic polymer in a Langmuir-Blodgett film. *J. Am. Chem. Soc.* **127,** 5788–5789 (2005).

19 Liu, J., Wang, J., Li, H., Shen, D., Zhang, J., Ozaki, Y. & Yan, S. Epitaxial crystallization of isotactic poly(methyl methacrylate) on highly oriented polyethylene. *J. Phys. Chem. B* **110,** 738–742 (2006).

20 Serizawa, T., Hamada, K., Kitayama, T. & Akashi, M. Recognition of stereoregular polymers by using structurally regulated ultrathin polymer films. *Angew. Chem. Int. Edn. Engl.* **42,** 1118–1121 (2003).

21 Serizawa, T., Hamada, K. & Akashi, M. Polymerization within a molecular-scale stereoregular template. *Nature* **429,** 52–55 (2004).

22 Hamada, K., Serizawa, T. & Akashi, M. Template polymerization using artificial double strands. *Macromolecules* **38,** 6759–6761 (2005).

23 Ajiro, H., Kamei, D. & Akashi, M. Methacrylic acid and methyl methacrylate oligomers adsorbed to porous isotactic poly(methyl methacrylate) ultrathin films and mechanistic studies of living template polymerization. *J. Polym. Sci., Part A: Polym. Chem.* **17,** 5879–5886 (2008).

24 Ajiro, H., Kamei, D. & Akashi, M. Macroporous silicagel substrate for stereoregular template polymerization of methacrylic acid using stereocomplex assembled thin films. *Polym. J.* **41,** 90–93 (2009).

25 Ajiro, H., Kamei, D. & Akashi, M. Mechanistic studies on template polymerization in porous isotactic poly(methyl methacrylate) thin films by radical polymerization and post-polymerization of methacrylate derivatives. *Macromolecules* **42,** 3019–3025 (2009).

26 Decher, G. Fuzzy nanoassemblies: toward layered polymeric multicomposites. *Science* **277,** 1232–1237 (1997).

27 Lohmeyer, J. H. G. M., Kransen, G., Tan, Y. Y. & Challa, G. Stereoassociation between poly(methyl methacrylate) and poly(methacrylic acid). *Polym. Lett. Edn.* **13,** 725–729 (1975).

28 Lohmeyer, J. H. G. M., Tan, Y. Y., Lako, P. & Challa, G. Stereoselective association between isotactic poly(methyl methacrylate) and syndiotactic poly(methacrylic acid). *Polymer* **19,** 1171–1175 (1978).

29 Serizawa, T., Hamada, K., Kitayama, T., Katsukawa, K., Hatada, K. & Akashi, M. Stepwise assembly of isotactic poly(methyl methacrylate) and syndiotactic poly(methacrylic acid) on a substrate. *Langmuir* **16,** 7112–7115 (2000).

30 Bosscher, F., ten Brinke, G. & Challa, G. Association of stereoregular poly(methyl methacrylates). 6. Double-stranded helical structure of the stereocomplex of isotactic and syndiotactic poly(methyl methacrylate). *Macromolecules* **15,** 1442–1444 (1982).

31 Kamei, D., Ajiro, H., Hongo, C. & Akashi, M. Dynamics of polymer chains in porous thin films prepared by layer-by-layer assembly of isotactic poly(methyl methacrylate) and syndiotactic poly(methacrylic acid). *Chem. Lett.* **37,** 332–333 (2008).

32 Kamei, D., Ajiro, H., Hongo, C. & Akashi, M. Solvent effects on isotactic poly(methyl methacrylate) crystallization and syndiotactic poly(methacrylic acid) incorporation in porous thin films prepared by stepwise stereocomplex assembly. *Langmuir* **25,** 280–285 (2009).

33 Kusy, R. P. Determination of the heat of fusion of isotactic poly(methyl methacrylate). *J. Polym. Sci., Part A: Polym. Chem.* **14,** 1527–1536 (1976).

34 Hatada, K., Ute, K., Tanaka, K., Kitayama, T. & Okamoto, Y. Preparation of highly isotactic poly(methyl methacrylate) of low polydispersity. *Polym. J.* **17,** 977–980 (1985).

35 Kitayama, T., He, S., Hironaka, Y., Iijima, T. & Hatada, K. Preparation of highly stereoregular poly(methacrylic acid) by stereospecific anionic polymerization of tri-methylsilyl methacrylate. *Polym. J.* **27,** 314–318 (1995).

36 Sauerbrey, G. The use of quarts oscillators for weighing thin layers and for microweighing. *Z. Phys.* **155,** 206–222 (1959).

37 Burton, Z. & Bhushan, B. Hidrophobicity, adhesion, and friction properties of nano-patterned polymers and scale dependence for micro- and nanoelectromechanical systems. *Nano Lett.* **5,** 1607–1613 (2005).

Supplementary Information accompanies the paper on Polymer Journal website (http://www.nature.com/pj)